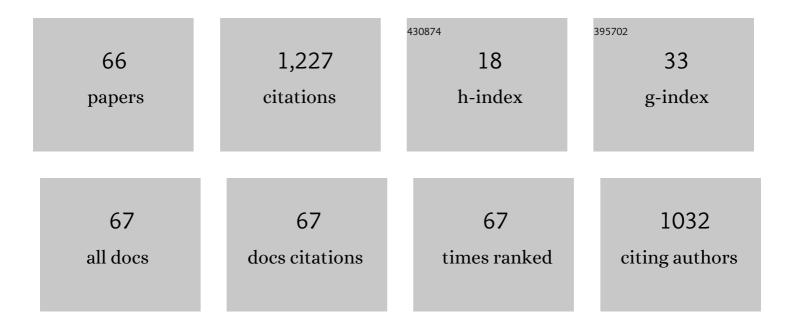
Yonghong He

List of Publications by Year in descending order

Source: https://exaly.com/author-pdf/2332824/publications.pdf Version: 2024-02-01



YONCHONG HE

#	Article	IF	CITATIONS
1	Programmable Broadband Responsive Lanthanideâ€Doped Nanoarchitecture for Information Encryption. Advanced Optical Materials, 2022, 10, 2101843.	7.3	7
2	A Self-Reference Interference Sensor Based on Coherence Multiplexing. Frontiers in Chemistry, 2022, 10, 880081.	3.6	3
3	Real-time monitoring the hydrolysis of chiral molecules by optical weak measurement. Optik, 2022, 263, 169340.	2.9	2
4	Specific detection of glucose by an optical weak measurement sensor. Biomedical Optics Express, 2021, 12, 5128.	2.9	3
5	Polarization Measurements and Evaluation Based on Multidimensional Polarization Indices Applied in Analyzing Atmospheric Particulates. Applied Sciences (Switzerland), 2021, 11, 5992.	2.5	9
6	In situ detection of electrochemical reaction by weak measurement. Optics Express, 2021, 29, 19292.	3.4	3
7	Optimization of the Weak Measurement System by Determining the Optimal Total Phase Difference. IEEE Photonics Journal, 2021, 13, 1-8.	2.0	0
8	High-Throughput Chiral Molecule Determination Based on Multi-Channel Weak Measurement. IEEE Photonics Journal, 2021, 13, 1-12.	2.0	1
9	Imaging Sensor for the Detection of the Flow Battery Via Weak Value Amplification. Analytical Chemistry, 2021, 93, 12914-12920.	6.5	7
10	Spectrum Intensity Ratio Detection for Frequency Domain Weak Measurement System. IEEE Photonics Journal, 2020, 12, 1-12.	2.0	3
11	Spectral-Domain Phase Microscopy for Thickness Encoded Suspension Array. IEEE Photonics Technology Letters, 2020, 32, 461-464.	2.5	0
12	Hydrogel-based microbeads for Raman-encoded suspension array using the reversed-phase suspension polymerization method and ultraviolet light curing. Analytical and Bioanalytical Chemistry, 2020, 412, 2731-2741.	3.7	2
13	Measuring angular rotation via the rotatory dispersion effect. Physical Review A, 2020, 102, .	2.5	5
14	A Waveguide-Coupled Surface Plasmon Resonance Sensor Using an Au-MgF2-Au Structure. Plasmonics, 2019, 14, 187-195.	3.4	12
15	Detection of Macromolecular Content in a Mixed Solution of Protein Macromolecules and Small Molecules Using a Weak Measurement Linear Differential System. Analytical Chemistry, 2019, 91, 11576-11581.	6.5	11
16	Gold-nanorod-enhanced Raman spectroscopy encoded micro-quartz pieces for the multiplex detection of biomolecules. Analytical and Bioanalytical Chemistry, 2019, 411, 5509-5518.	3.7	6
17	Detection of Simulated Periradicular Lesions in Porcine Bone by Optical Coherence Tomography. Journal of Endodontics, 2019, 45, 1024-1029.	3.1	3
18	Enhanced Interferometric Weak Value Amplification With Multiple Reflection. IEEE Photonics Technology Letters, 2019, 31, 1557-1560.	2.5	0

YONGHONG HE

#	Article	IF	CITATIONS
19	Fast and accurate decoding of Raman spectra-encoded suspension arrays using deep learning. Analyst, The, 2019, 144, 4312-4319.	3.5	27
20	A Differential Detection Method Based on a Linear Weak Measurement System. Sensors, 2019, 19, 2473.	3.8	1
21	Multifunctional weak measurement system that can measure the refractive index and optical rotation of a solution. Applied Physics Letters, 2019, 114, .	3.3	21
22	Label-free and Non-destruction Determination of Single- and Double-Strand DNA based on Quantum Weak Measurement. Scientific Reports, 2019, 9, 1891.	3.3	4
23	In situ mapping of activity distribution and oxygen evolution reaction in vanadium flow batteries. Nature Communications, 2019, 10, 5286.	12.8	45
24	Spectral-optical-tweezer-assisted fluorescence multiplexing system for QDs-encoded bead-array bioassay. Biosensors and Bioelectronics, 2019, 129, 107-117.	10.1	12
25	Dual-channel-coded microbeads for multiplexed detection of biomolecules using assembling of quantum dots and element coding nanoparticles. Analytica Chimica Acta, 2018, 1024, 153-160.	5.4	6
26	<i>In Situ</i> Diagnostics on the Dynamic Processes of Ash Deposit Formation, Shedding, and Heat Transfer in a Self-Sustained Down-Fired Furnace. Energy & amp; Fuels, 2018, 32, 4424-4431.	5.1	9
27	Effect of CO ₂ /H ₂ O on the Incipient Ultrafine Particulate Matter Formation in Oxy-fuel Combustion of High-Sodium Lignite. Energy & Fuels, 2018, 32, 4308-4314.	5.1	9
28	A chiral sensor based on weak measurement for the determination of Proline enantiomers in diverse measuring circumstances. Biosensors and Bioelectronics, 2018, 110, 103-109.	10.1	36
29	Scattering measurement of single particle for highly sensitive homogeneous detection of DNA in serum. Talanta, 2018, 178, 545-551.	5.5	6
30	Rapid Separation of Enantiomeric Impurities in Chiral Molecules by a Self-Referential Weak Measurement System. Sensors, 2018, 18, 3788.	3.8	5
31	A Fluidic Biosensor Based on a Phase-Sensitive Low-Coherence Spectral-Domain Interferometer. Sensors, 2018, 18, 3757.	3.8	4
32	Optical rotation based chirality detection of enantiomers via weak measurement in frequency domain. Applied Physics Letters, 2018, 112, .	3.3	41
33	Dual-spectra encoded suspension array using reversed-phase microemulsion UV curing and electrostatic self-assembling. RSC Advances, 2018, 8, 21272-21279.	3.6	4
34	Characterization on Ignition and Volatile Combustion of Dispersed Coal Particle Streams: <i>In Situ</i> Diagnostics and Transient Modeling. Energy & Fuels, 2018, 32, 9850-9858.	5.1	23
35	Determination of Tumor Marker Carcinoembryonic Antigen with Biosensor Based on Optical Quantum Weak Measurements. Sensors, 2018, 18, 1550.	3.8	11
36	Optimization of a quantum weak measurement system with its working areas. Optics Express, 2018, 26, 21119.	3.4	29

YONGHONG HE

#	Article	IF	CITATIONS
37	Monitoring microstructural variations of fresh skeletal muscle tissues by Mueller matrix imaging. Journal of Biophotonics, 2017, 10, 664-673.	2.3	60
38	Molecular imprinting sensor based on quantum weak measurement. Biosensors and Bioelectronics, 2017, 94, 328-334.	10.1	34
39	Digital immunoassay of a prostate-specific antigen using gold nanorods and magnetic nanoparticles. RSC Advances, 2017, 7, 27595-27602.	3.6	17
40	Digital triplex DNA assay based on plasmonic nanocrystals. Analytical and Bioanalytical Chemistry, 2017, 409, 3657-3666.	3.7	4
41	Nondisturbing transverse acoustic sensor based on weak measurement in Mach–Zehnder interferometer. Optical Engineering, 2017, 56, 034107.	1.0	4
42	Enhancement of short coherence digital holographic microscopy by optical clearing. Biomedical Optics Express, 2017, 8, 2036.	2.9	1
43	Optical demodulation system for digitally encoded suspension array in fluoroimmunoassay. Journal of Biomedical Optics, 2017, 22, 1.	2.6	1
44	Optical weak measurement system with common path implementation for label-free biomolecule sensing. Optics Letters, 2016, 41, 5409.	3.3	52
45	Temperature-Regulated Surface Plasmon Resonance Imaging System for Bioaffinity Sensing. Plasmonics, 2016, 11, 771-779.	3.4	14
46	Digital barcodes of suspension array using laser induced breakdown spectroscopy. Scientific Reports, 2016, 6, 36511.	3.3	11
47	Digital Concentration Readout of DNA by Absolute Quantification of Optically Countable Gold Nanorods. Analytical Chemistry, 2016, 88, 10994-11000.	6.5	24
48	Retardance of bilayer anisotropic samples consisting of well-aligned cylindrical scatterers and birefringent media. Journal of Biomedical Optics, 2016, 21, 055002.	2.6	8
49	The detection method for small molecules coupled with a molecularly imprinted polymer/quantum dot chip using a home-built optical system. Analytical and Bioanalytical Chemistry, 2016, 408, 5261-5268.	3.7	10
50	Application of quantum weak measurement for glucose concentration detection. Applied Optics, 2016, 55, 1697.	2.1	46
51	Quantum-dots-encoded-microbeads based molecularly imprinted polymer. Biosensors and Bioelectronics, 2016, 77, 886-893.	10.1	48
52	Quantitatively differentiating microstructures of tissues by frequency distributions of Mueller matrix images. Journal of Biomedical Optics, 2015, 20, 105009.	2.6	51
53	Qualitative Analysis of Cross-Border E-Commerce Based on Transaction Costs Theory. , 2015, , .		7
54	Optical waveguide sensor based on silica nanotube arrays for label-free biosensing. Biosensors and Bioelectronics, 2015, 67, 230-236.	10.1	18

YONGHONG HE

#	ARTICLE	IF	CITATIONS
55	Study on the Despeckle Methods in Angular Surface Plasmon Resonance Imaging Sensors. Plasmonics, 2015, 10, 729-737.	3.4	7
56	Microfluidic generation of uniform quantum dot-encoded microbeads by gelation of alginate. RSC Advances, 2015, 5, 62706-62712.	3.6	16
57	Noninvasive and Real-Time Plasmon Waveguide Resonance Thermometry. Sensors, 2015, 15, 8481-8498.	3.8	6
58	Decoding of Quantum Dots Encoded Microbeads Using a Hyperspectral Fluorescence Imaging Method. Analytical Chemistry, 2015, 87, 5286-5293.	6.5	25
59	Characterizing microstructures of cancerous tissues using multispectral transformed Mueller matrix polarization parameters. Biomedical Optics Express, 2015, 6, 2934.	2.9	104
60	Fabrication and optical sensing properties of mesoporous silica nanorod arrays. RSC Advances, 2015, 5, 90659-90666.	3.6	16
61	CHARACTERISTIC FEATURES OF MUELLER MATRIX PATTERNS FOR POLARIZATION SCATTERING MODEL OF BIOLOGICAL TISSUES. Journal of Innovative Optical Health Sciences, 2014, 07, 1350028.	1.0	12
62	Study on retardance due to well-ordered birefringent cylinders in anisotropic scattering media. Journal of Biomedical Optics, 2014, 19, 065001.	2.6	11
63	Characterizing the microstructures of biological tissues using Mueller matrix and transformed polarization parameters. Biomedical Optics Express, 2014, 5, 4223.	2.9	167
64	A SiO ₂ -coated nanoporous alumina membrane for stable label-free waveguide biosensing. RSC Advances, 2014, 4, 62987-62995.	3.6	9
65	Mapping local orientation of aligned fibrous scatterers for cancerous tissues using backscattering Mueller matrix imaging. Journal of Biomedical Optics, 2014, 19, 106007.	2.6	73
66	Multichannel, Line-Monitoring Sensing Approach Based on Long-Range Surface Plasmons. Plasmonics, 2014, 9, 513-518.	3.4	0